# Eumelanin, from the Molecular State to Film

Manuel Reali[1], Anthony Camus[1], Guillaume Beaulieu[1], Jordan De Angelis[2], Christian Pellerin[3], Alessandro Pezzella[4], Clara Santato[*1]

[1]Department of Engineering Physics, Polytechnique Montreal, C.P. 6079, Succ. Centre-ville, Montréal, QC, H3C 3A7, Canada

[2]Department of Electronic, Electrical and Information Engineering (DEI), University of Bologna, Viale del Risorgimento 2, 40136, Italy

[3]Département de chimie, Université de Montréal, C.P. 6128, Succ. Centre-ville, Montréal, QC, H3C 3J7, Canada

[4]Department of Physics "Ettore Pancini", University of Naples "Federico II", Complesso Universitario Monte S. Angelo, Via Cintia 1, 80126, Naples, Italy.

*Clara Santato (Email: clara.santato@polymtl.ca)

*Keywords* Eumelanin, (5,6)-dihydroxyindole (DHI), (5,6)-dihydroxyindole-2-carboxylic acid (DHICA), self-assembly, polymerization, films

**ABSTRACT** Eumelanin, a macromolecular biopigment, is an attractive candidate for Sustainable (Green) Organic Electronics. Establishing structure-property relationships in eumelanin films is an essential step to exploit its technological potential. We report on the evolution from the molecular state to film after spin coating on silicon dioxide solutions of (5,6)-dihydroxyindole (DHI) and (5,6)-dihydroxyindole-2-carboxylic acid (DHICA) eumelanin building blocks (monomers). The evolution of the spin-coated films was followed under various environmental conditions, such as ambient vs ammonia atmosphere which catalyzes polymerization. Atomic force microscopy images reveal dramatic morphological changes as a function of the environmental conditions. Infrared and UV-Vis spectroscopies indicate these changes are due to a combination of physical (self-assembly) and chemical (polymerization) processes. Preliminary electrical measurements on films were also carried out.

## 1. INTRODUCTION

The expansion of consumer electronics has generated unsustainable amounts of Waste Electric & Electronic Equipment (WEEE), posing serious environmental and health concerns[1]. Sustainable Organic Electronics, based on the use of abundant, bio-sourced and biodegradable organic electronic materials, are an emerging route to design low eco- and human-toxicity technologies and alleviate the environmental footprint of electronics[2,3]. Despite their interest, enormous challenges have to be overcome before applying bio-sourced organic materials in electronics.

The charge transfer and transport properties of bio-sourced organic materials are complex, due to the materials' chemical composition and structure. Indeed, they are usually immersed in aqueous saline media, such that their composition includes water and salts. Furthermore, their biosynthesis brings about a certain amount of chemical disorder (chemical heterogeneity), e.g. macromolecules resulting from more than one building block (monomer), and physical disorder, e.g. π-π stacked regions with different extension and orientation coexisting in the supramolecular structure of the materials[4–7]. Intrinsic chemical and physical disorder (that we qualify as intermediate since these materials are not well ordered , yet not amorphous either[8]), are among the key factors limiting the performance of corresponding devices (e.g. in terms of charge carrier mobility).

Considering the weak van der Waals interactions that bind organic molecules together into films**,** polymorphism (i.e. lack of a unique structure due to different types of molecular arrangements) has always been a challenge when attempting to establish sound structure-property relationships in organic electronic materials and optimize device performance [9,10].

Among bio-sourced materials, eumelanin, a black-brown bio-pigment belonging to the melanin family, is an interesting candidate for study[11–14]. Eumelanin is a redox-active quinone-based bio-macromolecule that features an electronically conjugated molecular structure (alternating single and double bonds). It is derived from the oxidative polymerization of 5,6-dihydroxyindole (DHI) and 5,6-dihydroxyindole-2-carboxylic acid (DHICA) monomers (building blocks)[15] (Scheme 1). The building blocks have several polymerization sites and co-exist in different redox states (fully reduced hydroquinone (HQ), semi-reduced semiquinone (SQ), and fully oxidized quinone (Q)). It, therefore, features chemical heterogeneity. Considering the different supramolecular structures that can be generated from different monomers and oligomers, eumelanin also features physical (structural) disorder[16–18]. A few models predict that ensembles of oligomers of the two building blocks hierarchically build up via π-π stacking with inter-plane distance of about 3.4 Å and lateral extension of about 20 Å[19–24].

Recently, chemically controlled films obtained from eumelanin building blocks have been fabricated using an ammonia-induced (catalyzed) solid-state polymerization (AISSP)[25,26].

Understanding the formation of DHI- and DHICA-based films, as determined by both chemical (covalent) and physical (self-assembly) interactions, is needed to establish structure-functional properties relationships, a crucial piece of knowledge in view of the practical applications of eumelanin films in electronics.

In this work, we report on the early stages of the formation of films obtained from eumelanin building blocks under different environmental conditions (ambient conditions vs ammonia atmosphere, laboratory daylight vs dark). Atomic force microscopy (AFM) and optical microscopy (OM) images were acquired at different stages of film formation. Infrared spectroscopy (IR) and UV-Vis spectroscopy surveys showed that the formation of DHI- and DHICA-based films is driven by the interplay of physical (self-assembly) and chemical (covalent) interactions. Preliminary investigations into the electrical properties of the films were also carried out.

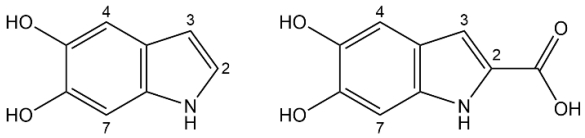


**Scheme 1.** Molecular structure of 5,6-dihydroxyindole (DHI) and 5,6-dihydroxyindole-2-carboxylic acid (DHICA) eumelanin building blocks**.**

## 2. EXPERIMENTAL

Preparation of Chemically Controlled DHI- and DHICA-based Films. DHI and DHICA powders were synthesized as previously reported[46]. Ten milligrams of DHI and DHICA powders were dissolved in 1 ml anhydrous methanol in controlled atmosphere ($N_2$ with $O_2$ and $H_2O$ < 5 ppm). DHI and DHICA solutions were spin-coated (40 µL, 30 s at 2000 rpm) on $SiO_2$ /Si (1 cm × 1 cm, (1-0-0) n-doped Si, $SiO_2$ thickness of 200 ± 10 nm) for morphological and electrical characterization, on fused silica substrates (pre-cleaned, area 1 cm × 1 cm, thickness 0.96-1.06 mm) for optical characterization and $BaF_2$ windows for IR characterization. Prior to spin coating, substrates were cleaned by sequential sonication in acetone, isopropanol and deionized water, followed by 10 min UV-ozone treatment. Films were exposed to different environmental conditions after spin coating: (i) AC-L-DHI and AC-L-DHICA films stored in ambient conditions (relative

humidity (RH) between 30% and 50%) and exposed to ambient laboratory daylight (Philips, F32T8/TL841 model, 32 W); (ii) AC-D-DHI and AC-D-DHICA films stored at ambient conditions in the dark (between 30 %RH and 50 %RH). AC-L films were kept in open sample holders whereas AC-D films were kept in closed sample holders, wrapped up in aluminum foil; (iii) AISSP-L-DHI, AISSP-D-DHI, AISSP-L-DHICA and AISSP-D-DHICA films exposed to ammonia vapors (Sigma Aldrich, 28-30% w/v) at ambient conditions for 24 h. AISSP-L- and AISSP-D- films were exposed to ammonia vapors in a glass bell respectively unprotected and protected from laboratory daylight. To protect AISSP-D- samples from laboratory daylight, an aluminum foil was used to cover the glass bell.

Powders were synthesized in the Department of Chemical Sciences of the University of Naples, "Federico II" (Italy) and stored in closed vials (under $N_2$, protected by Parafilm®) during shipping to Polytechnique Montreal. After shipping vials were stored at -25 °C.

Morphology. Morphology of DHI and DHICA films on $SiO_2$/Si substrates was investigated at ambient conditions using AFM in tapping mode (AFM Digital Instruments Dimensions 3100, aluminum-coated silicon cantilever (radius 10 nm, spring constant 42 N $m^{-1}$)). AFM images were analyzed using NanoScope Analysis software.

In the case of DHI films, the formation rate of the fern front was evaluated by taking the difference between two sequential front positions of a forming fern along its $\hat{\mathbf{x}}$ direction (yellow arrow, Figure 1 (a)). The width of the ferns' branches as a function of time was evaluated by taking the average width of a fern along its $\hat{\mathbf{y}}$ direction (blue arrow, Figure 1 (a)). Our fabrication protocol enables a well reproducible morphology of AC-DHI films (90% over 100 experiments). Furthermore, our protocol gives an average of about 10 spiral-like shapes of AC-DHI films on $SiO_2$.

For AC-L-DHICA, the formation rate of rod-shaped structures along the $\hat{\boldsymbol{z}}$ direction ($v_z(t)$, Table S2, SI) was evaluated from the time derivative of the average height profile of the rods (z(t), Table S2, SI). The fabrication protocol provides a well reproducible morphology and surface coverage of AC-L-DHICA films (90% over 50 experiments).

Fourier Transform Infrared Spectroscopy. IR spectra were acquired in inert dry air in transmission mode using a Vertex 70 FT-IR spectrometer (Bruker Optics) equipped with a DLaTGS detector. The background spectra of the atmosphere were automatically removed from the actual spectra during the measurements. Spectra were recorded with 4 $cm^{-1}$ resolution by averaging 200 scans.

UV-Visible Absorption Spectroscopy. UV-Vis spectra of DHI and DHICA were collected using a Cary 7000 Universal Measurement Spectrophotometer (Agilent, UMS). The total transmitted (%T) and reflected (%R) radiation was collected to evaluate the total resulting absorption of the films by posing $\%A = 100 - (\%T + \%R)$. The Tauc plot model was used to extract the optical absorption gap of DHI and DHICA films from the linear extrapolation of the plot $(\alpha h\nu)^{1/2}$ vs hν, where α is the absorption coefficient, h the Planck's constant and ν the frequency of the light. The wavelength-dependent absorption coefficient was computed by posing $\alpha(\lambda) = \%A/_t$, where $t$ is the thickness of the film. The thickness was evaluated by means of a profilometer tip after gently scratching the films.

IR and UV-Vis spectra were acquired on different films prepared under similar conditions at least in duplicate.

Electrical characterization. Organic films were deposited on $SiO_2$/Si substrates photolithographically patterned with interdigitated circular electrodes (5 nm of Ti adhesion layer, 40 nm of Au) with interelectrode distance $L = 10\ \mu$m and electrode width $W = 24.5$ mm and total in-plane area $A = 0.8$ $mm^2$ (Figure 5 (a)). Films were transferred in a manipulated cryogenic optoelectronic probe station (CXP, Lakeshore). Current-voltage measurements were acquired using Agilent B1500 in vacuum ($10^{-7}$-$10^{-8}$ Torr, 295 K).

The electrical conductivity as a function of voltage scan rate was evaluated as follows:

$$\sigma = \frac{L}{A * R}$$

where $R$ is the film resistance (including the contact resistance) evaluated at a voltage $V = 1.5\ V$.

The charge stored vs. voltage scan rates was calculated as follows:

$$q = \frac{\int_{V_m}^{V_M} I(V')dV'}{(\frac{dV}{dt})}$$

where $V_M$ and $V_m$ are voltage extremities of the hysteresis characteristics, $\Delta V = V_M - (-V_m)$ the voltage window and $\frac{dV}{dt}$ the voltage scan rate.

The ρ-V characteristics of AC-L-DHICA and AC-L-DHI films were obtained by evaluating the differential resistance $\boldsymbol{R(V)} = (\frac{\boldsymbol{dI}}{\boldsymbol{dV}})^{\boldsymbol{-1}}$ (namely the inverse of the derivative of the hysteresis current with respect to the hysteresis voltage) and then by plotting the resistivity $\boldsymbol{\rho(V)} = \frac{\boldsymbol{A*L}}{\boldsymbol{R(V)}}$ as a function of the voltage.

## 3. RESULTS AND DISCUSSION

### Atomic Force Microscopy (AFM) Characterization

#### DHI-based films in dark conditions: changes during the first few hours

AFM images of spin-coated DHI samples exposed to ambient conditions (indicated as AC, Table 1) in the dark (indicated as D) reveal the formation of *fern-like* structures (green dashed lines in region A, Figure 1 (a)), within a few hours of deposition.

We followed the growth of the ferns in the $\hat{x}$ direction and found that the growth rate is about 5 μm $min^{-1}$ during the first hour, decreasing to about 0.5 μm $min^{-1}$ in 3 h (see Experimental). Within this time, the fern-like structures are about 120 nm high and branches are about 400 nm wide (Figure 1 (a), red and blue crosses). Optical microscopy images, acquired a few hours after preparation, show that fern-like structures are part of spiral-like shapes forming on the surface (Scheme S1 (a) supplementary information, SI). After about 3 h, spiral-like shapes are approximately 200 μm×150 μm (e.g. Scheme S1 (a) and (f), SI). The density of the ferns depends on the distance from the center of the spiral. Denser branches are observed close to the center (Scheme S1 (b) and (c), SI).

The formation of fern-like structures likely results from diffusion-limited aggregation (DLA)[27] paralleled by the *coffee ring effect*[28]. Indeed, DLA has already been observed during the self-assembly of natural and synthetic melanin particles in aqueous solutions[29,30]. During DLA, particles follow a Brownian motion with the probability to stick on the first encountered cluster being higher than that of sticking on the inner portions. Thus, the outermost portions of the clusters screen the innermost ones, leading to the formation of branched structures. In the coffee ring effect, ring-like structures (like our spiral-like shapes) generate at the micrometric scale after the evaporation of solvent drops. Different evaporation rates across the spin-coated sample cause an outward flow of solvent to minimize surface tension bringing about accumulation of particles at the edge of the forming structures.

#### DHI-based films stored in open sample holders in the presence of laboratory daylight: changes during the first few hours

AFM images of DHI films exposed to ambient conditions, stored in open sample holders in the presence of laboratory daylight (indicated as L, Table 1 and Experimental) show, during the first few hours after deposition, the formation of fern-like structures as did their dark counterparts. On top of fern-like structures, *pillar-like aggregates* form (Figure 1 (b), region B and Figure S1, SI).

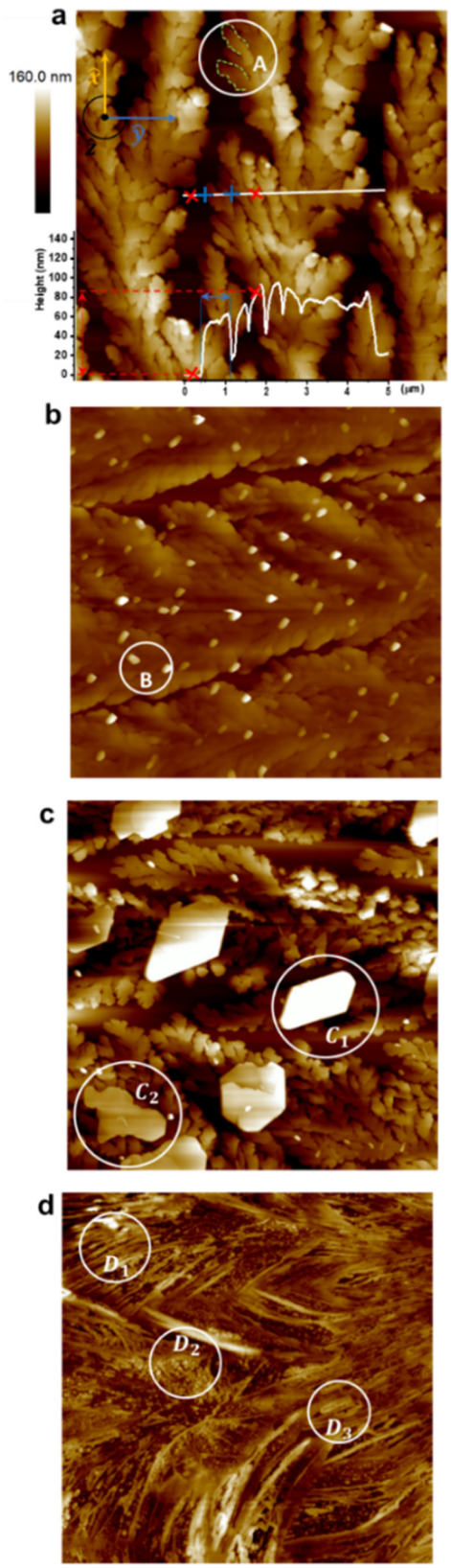


**Figure 1**. 10 μm×10 μm AFM height images of **(a)** AC-D-DHI films acquired after 3 h **(b)** AC-L-DHI after a few minutes and **(c)** AC-L-DHI after one day. In **(d)** AISSP-L-DHI film after one day.

The density of the pillar-like aggregates is between 0.5 and 1 $\mu m^{-2}$. These aggregates grow in the $\hat{z}$ direction at a rate of about 70 nm $h^{-1}$. Within 1-2 h of exposure to laboratory daylight, pillar-like aggregates reach a height and width of about 150 nm and 400 nm, respectively. Heights and widths of pillar-like aggregates did not significantly change after about 2 h from the exposure to laboratory daylight.

### DHI-based films stored in open sample holders, in the presence of laboratory daylight: changes from one day to one month

After about one day at ambient conditions, in open sample holders, under laboratory daylight, well-defined structures (*crystal-like aggregates)* are observable on the ferns (Figure 1 (c), regions $C_1$ and $C_2$). These aggregates, possibly developing from pre-existing pillar-like aggregates, grow in the $\hat{z}$ direction at an initial rate of about 25 nm $h^{-1}$. The process is considered completed about 30 h after deposition (Table S1, SI). No further drastic morphological changes were observed during the following month.
Our films were processed from anhydrous methanol solutions, in dry nitrogen. Other morphologies have been reported in the literature for non-anhydrous processing conditions[25,26]. This observation points to the potentially relevant role played by moisture in affecting film morphologies.

### Ammonia-Induced Solid-State Polymerized-DHI-based (AISSP-DHI) Films

AISSP-L-DHI films feature remarkable polymorphism. AFM images show that films feature fibrous morphology with a small population of *small spheres* and *flat rings* (Figure 1 (d), regions $D_1$, $D_2$ and $D_3$ respectively, Table 1 and Experimental). These structures reach a height of about 100 nm after one day. Upon exposure to ambient conditions, the height of these structures did not significantly increase. While following the sample for a month, we did not observe any further morphological changes.

AFM images of AISSP-D-DHI films (Figure S2, SI), show spontaneous segregation into spherical aggregates confined by rims (Figure S2 (a) and (b), SI). These structures could result from the interplay of intermolecular and film-substrate van der Waals interactions possibly associated to thermodynamic instabilities in the films, leading to de-wetting-like processes[31].

### DHICA-based films stored in open sample holders, in the presence of laboratory day light: changes during the first few hours

AFM images of DHICA spin-coated samples exposed to ambient conditions and laboratory daylight show *rod-shaped structures*[15], which form on the surface already in the early stages of formation (about 1 h from fabrication, Figure 2 (a)). After about 1 h, rod height and width are about 70 nm and 180 nm, respectively. Over one month, rod height and width increase to about 100 nm and 300 nm, respectively (Figure 2, Figure S3 (red and blue crosses) and Table S2, SI). Rod density reaches a maximum after about one week and a minimum after about one month (Figure 2 (e)), likely due to Ostwald ripening[32]. The formation of larger rods ((Figure 2 (d) region $D_1$, $D_2$) is paralleled by a change in the root mean square roughness ($R_{RMS}$) of the films from about 15 nm to about 65 nm (Table S2, SI)[33]. The decrease of the rods' density does not affect the homogeneity of the rods on the surface; substrate coverage is still very uniform even one month from fabrication. It is worth noticing that AFM images of DHICA films spin-coated at ambient conditions in dark (AC-D-DHICA, Table 1) feature the same morphology of their counterparts exposed to laboratory daylight (Figure S4 (a), SI).

### Ammonia-Induced Solid-State Polymerized-DHICA based (AISSP-DHICA) films

AISSP-L-DHICA films are polymorphic as were their DHI counterparts. AFM images show that films feature layers made of *small spheres* on which *rods* and *shell-like structures* developed at high density (Figure 2 (f), regions $F_1$, $F_2$ and $F_3$ respectively). The morphology of AISSP-L-DHICA films does not evolve over time, as we also observed for AISSP-DHI films (Figure 1 (d)).

DHICA films exposed to ammonia vapors in dark (AISSP-D-DHICA, Table 1) are not polymorphic as were their counterparts exposed to laboratory daylight. AFM images of AISSP-D-DHICA samples show dense aggregates, about 50 nm high (Figure S4 (b), SI). Likely, the exposure of AISSP-DHICA samples to light favors the formation of different molecular aggregates that generate the observed polymorphism.

### Chemical Characterization

The changes in DHI-and DHICA-based samples was observed by IR spectroscopy. Indeed, molecular vibrational modes can provide information about the physical (self-assembled) state and chemical (monomeric or polymerized) state in the films [34,35].

**Table 1.** Experimental conditions for the study of DHI- and DHICA-based samples on $SiO_2$. The abbreviations AC-L and AC-D respectively indicate films formed at ambient conditions with and without exposure to laboratory daylight, while AISSP-L and AISSP-D represent their counterparts exposed to ammonia vapors.

| Name | Storage environment | | Light conditions | | Morphology observed | Time of observation |
|---|---|---|---|---|---|---|
| | Air | Ammonia vapors | Light | Dark | | |
| DHI | | | | | | |
| AC-L-DHI | × | | × | | Fern-like | 0-3 h |
| | | | | | Pillar-like | 1-3 h |
| | | | | | Crystal-like | 20-30 h |
| AC-D-DHI | × | | | × | Fern-like | 0-3 h |
| AISSP-L-DHI | | × | × | | Fibers, sphere-like, continuous flat regions | 24-26 h |
| AISSP-D-DHI | | × | | × | Spherical-like shapes confined by rims | |
| DHICA | | | | | | |
| AC-L-DHICA | × | | × | | Rod-shaped | 0-3 h |
| AC-D-DHICA | × | | | × | Rod-shaped | 0-3 h |
| AISSP-L-DHICA | | × | × | | Small spheres, shell-like and rods | 24-26 h |
| AISSP-D-DHICA | | × | | × | Dense aggregates | 24-26 h |

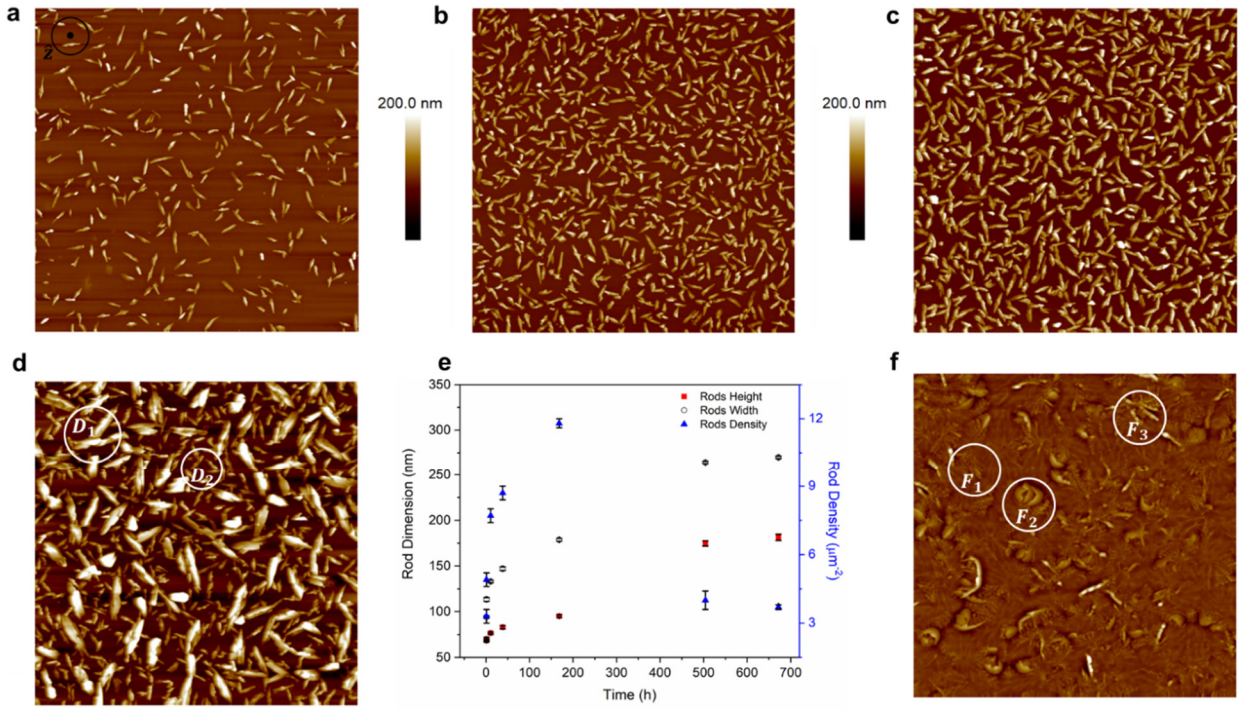


**Figure 2.** 10 μm×10 μm AFM height images of AC-L-DHICA samples acquired at about **(a)** 1 h, **(b)** 1 d, **(c)** 3 d and **(d)** 1 week. In **(e)** Rod Dimension (average Rod Height and Rod Width) and Rod Density of AC-L-DHICA samples as a function of time. In **(f),** AISSP-L-DHICA sample after one day.

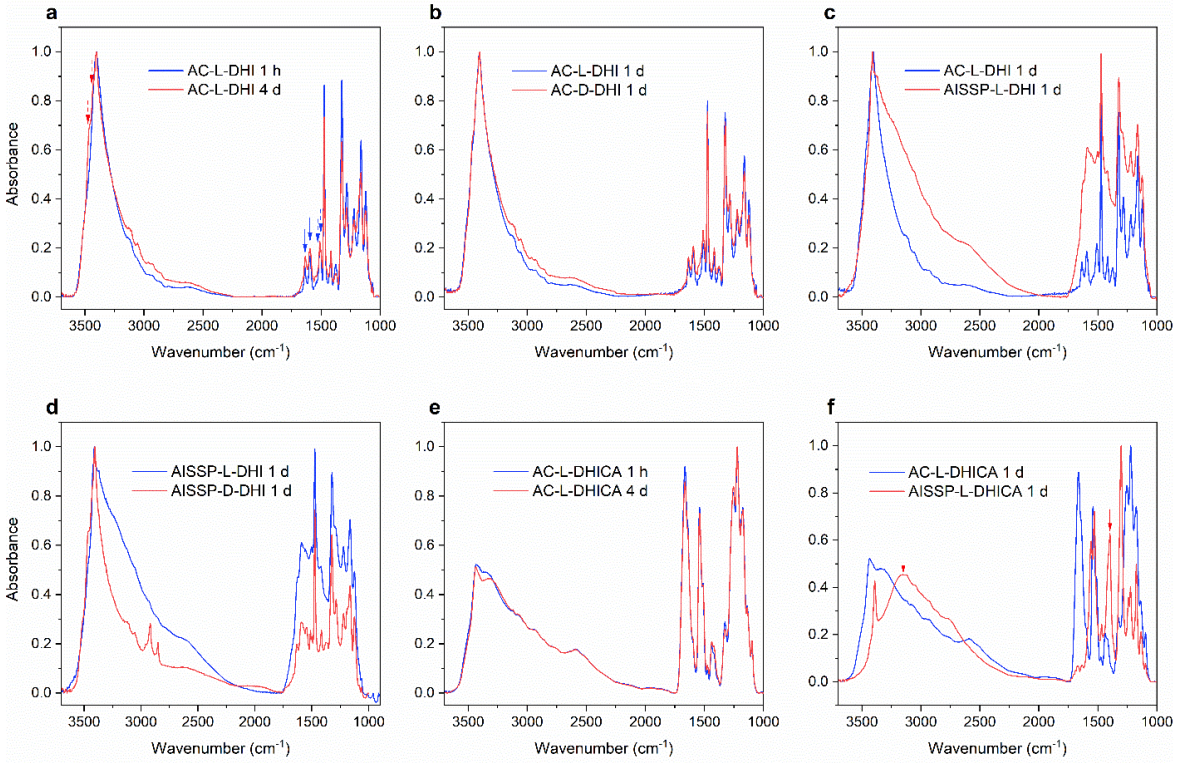


**Figure 3.** IR spectra of **(a)** AC-L-DHI films at different stages of formation. IR spectra of **(b)** AC-L-DHI and AC-D-DHI, **(c)** AC-L-DHI and AISSP-L-DHI and **(d)** AISSP-L-DHI and AISSP-D-DHI after one day. IR spectra of **(e)** AC-L-DHICA films at different stages of formation. IR spectra of **(f)** AISSP-DHICA and AISSP-L-DHICA films acquired after one day. DHI spectra were normalized to the O-H stretching band peak (3400 $cm^{-1}$) while DHICA spectra were normalized to the maximum peak (ca. 1300 $cm^{-1}$). For further details on abbreviations see Table 1 and experimental section.

## AC-DHI based films: changes in IR spectra

The IR spectrum of AC-L-DHI films about 1 h after fabrication is characteristic of the monomeric form of DHI[34,35]. It features a strong broadband around 3400 $cm^{-1}$ due to O-H stretching vibrations (Figure 3(a)) that overlap with the N-H stretching with various levels of hydrogen bonding. The aliphatic C-H stretching modes expected within 2934-2837 $cm^{-1}$ are mostly obscured. Two peaks, at 1636 $cm^{-1}$ and at 1595 $cm^{-1}$, stem from C=C vibrations in the phenyl and pyrrole rings, while two features at 1507 $cm^{-1}$ and 1473 $cm^{-1}$ are due to coupled in-plane ring and C-H deformation modes (Figure 3(a), blue solid and dashed arrows respectively). Additional groups of peaks attributed mainly to C-H and O-H deformations, are present at 1380-1120 $cm^{-1}$. We do not observe any band in the carbonyl stretching region (1715-1660 $cm^{-1}$) of the spectrum at 1 h.

After 4 days (4 d, indicated in red), two shoulders appear at around 3460 $cm^{-1}$ and 3430 $cm^{-1}$ (Figure 3(a), red dashed arrows). This points to a possible preferential supramolecular arrangement developing in the samples. Indeed, band splitting is an indication of the existence of specific molecular environments within the sample and is typically observed upon crystallization of initially amorphous materials. There is also a small increase of the intensity of the background around 1750-1600 $cm^{-1}$ that can be associated with the formation of carbonyl groups by oxidation.

The formation of carbonyl bands in DHI melanin is attributable to the oxidation of the hydroquinone form into the semiquinone and quinone forms [35,36]. Thus, the observed slight increase of intensity in the carbonyl region of the 4 d spectrum suggests slow oxidation of DHI films at ambient conditions. All in all, a reorganization of DHI via noncovalent interactions (supramolecular assembly) is observed as a function of time. It is possible that the formation of pillar-like and crystal-like aggregates, observed by AFM (Figure 1 (b) and (c)), is related to supramolecular self-assembly manifested by the splitting of the 3400 $cm^{-1}$ band. The IR spectrum of AC-D-DHI films after one day is akin to that of AC-L-DHI, except for a slightly broader O-H stretching band (Figure 3(b)).

## AISSP-DHI based films: changes in IR spectra

The IR spectrum of AISSP-L-DHI films after one day (1 d) displays a much broader O-H and N-H stretching band compared to AC-L-DHI (Figure 3 (c)). The absorption of AISSP-L-DHI films in the carbonyl region is also stronger than that of AC-L-DHI films. These observations indicate that samples exposed to ammonia are more oxidized than those stored at ambient conditions. Oxidation of

hydroquinone (HQ) is a fundamental step towards achieving the polymerization of DHI[15,19,37,38].

It is worth noticing that the absence of splitting around 3400 $cm^{-1}$ in the IR spectrum of AISSP-L-DHI could be linked to the lack of pillar-like and crystal-like aggregates in their AFM morphology (Figure 1 (d)).

The spectrum of AISSP-D-DHI after one day is quite different from that of AISSP-L-DHI (Figure 3 (d)). In particular, the strong band around 3400 $cm^{-1}$ is narrower and the broad absorption in the carbonyl region is lower than for its counterpart exposed to laboratory daylight (AISSP-L-DHI), pointing to a lower extent of the oxidation. Furthermore, the band around 3400 $cm^{-1}$ shows the same shoulders as noted in Figure 3 (a) for the AC-L-DHI films prepared in absence of ammonia and attributed to a preferential supramolecular arrangement.

### DHICA-based films: changes in IR spectra

The IR spectrum of AC-L-DHICA shows an O-H band at 3437 $cm^{-1}$ a shoulder at around 3346 $cm^{-1}$ as well as a strong C=O band at 1660 $cm^{-1}$. Furthermore, the IR spectrum of DHICA samples feature more intense absorption around 1200 $cm^{-1}$ than does AC-L-DHI, this last attributable to additional C-O stretching (Figure S5 (a), SI). The appearance of these bands in the IR spectrum of AC-L-DHICA stems from the anticipated presence of carboxylic acid groups in DHICA. The IR spectra of AC-L-DHICA, recorded after 1 h and 4 d, do not significantly change, except for the appearance of a more defined shoulder at 3346 $cm^{-1}$ (Figure 3(e)).

The IR spectrum of AC-D-DHICA films after one day is akin to that of AC-L-DHICA, except for a more intense band at 3437 $cm^{-1}$ and a broader O-H shoulder at about 3346 $cm^{-1}$ (Figure S5 (b)). The region of the carbonyl band, for both AC-L-and AC-D-DHICA samples, is almost unchanged after 4 d*, indicating very limited oxidation* within this time (respectively Figure 3(e) and Figure S5 (c), SI).

The spectrum of AISSP-L-DHICA films after 1 d, is considerably different from that of AC-L-DHICA counterparts. We observe the appearance of a new band in the spectrum of AISSP-L-DHICA at 3151 $cm^{-1}$ (red solid arrow, Figure 3(f)). The C=O peak at 1660 $cm^{-1}$ of carboxylic acid groups, found for AC-L-DHICA, is absent in the spectrum of AISSP-L-DHICA. In the region of C=C vibrations of AISSP-L-DHICA spectrum, the peak at 1545 $cm^{-1}$ is replaced by two peaks located at 1557 $cm^{-1}$ and 1529 $cm^{-1}$. This process is paralleled by the appearance of strong peaks at about 1300 $cm^{-1}$ and 1400 $cm^{-1}$ and the weakening of the peaks at 1253 $cm^{-1}$ and 1222 $cm^{-1}$.

The IR spectrum of AISSP-D-DHICA after 1 d is similar to that of AISSP-L-DHICA, except for a slightly broader band at 3151 $cm^{-1}$, a weaker peak at about 1300 $cm^{-1}$ and two stronger ones at about 1557 $cm^{-1}$ and 1529 $cm^{-1}$ (Figure S5 (d), SI).

One plausible explanation for these observations is an acid-base reaction between ammonia and the carboxylic group of DHICA. Ammonia can act as proton acceptor when in proximity with the carboxylic acid groups of DHICA in AISSP-DHICA samples. The formation of an ammonium salt could explain the appearance of the broad absorption band at 3150 $cm^{-1}$, the new intense band at 1400 $cm^{-1}$ (Figure 3 (f) and Figure S5 (d), red and blue solid arrows respectively, SI) and the shift of the C=O stretching band to lower frequencies in the carboxylate form.

The deprotonation process reveals the different role played by ammonia in film formation from DHI and DHICA. AISSP-DHI films are more oxidized than their ambient conditions counterparts. Our results suggest that, for L- and D-DHICA, ammonia plays a predominant role as acid-base agent, not catalyst.

### UV-Vis spectra of DHI and DHICA-based films

The UV-Vis spectrum of AC-L-DHI films after about 1 h from fabrication shows a broad peak with lambda max of about 307 nm (Figure 4(a)). In a timescale of one week (7 d) at ambient conditions, the peak at 307 nm is more intense than after 1 h and 1 d. The UV-Vis spectrum of AC-L-DHICA films after 1 h shows a broad peak located at lambda max of 364 nm (Figure 4(b)). The UV-Vis spectra of AC-L-DHICA films also undergo changes over time. After one week at ambient conditions, the peak shifts to lambda max of 359 nm and its width increases. The UV-Vis spectra of AISSP-L-DHI films are broadband and do not significantly change within one week of observation (Figure 4 (c), Table S3). Conversely, spectra of AISSP-L-DHICA show a small feature at around 351 nm (Figure 4 (d) and Table S3). As in the case of AISSP-L-DHI, we did not observe any remarkable variation of the absorption spectra of AISSP-L-DHICA in the timeframe of one week.

The progressive increase of optical absorption in the visible region of the spectrum, for both AC-L-DHI and AC-DHICA, might stem from an improvement of π-electron delocalization through self-assembly[39–41]. To validate this conjecture, we evaluated the highest occupied molecular orbital (HOMO)-lowest unoccupied molecular orbital (LUMO) optical energy gap of our films using the *Tauc Plot model*[13] (see Experimental and Table S3, SI). The evolution of the optical HOMO-LUMO energy gap of both AC-L-DHI and AC-L-DHICA films, after one week at ambient conditions, cannot exclude the hypothesis of π-electron delocalization.

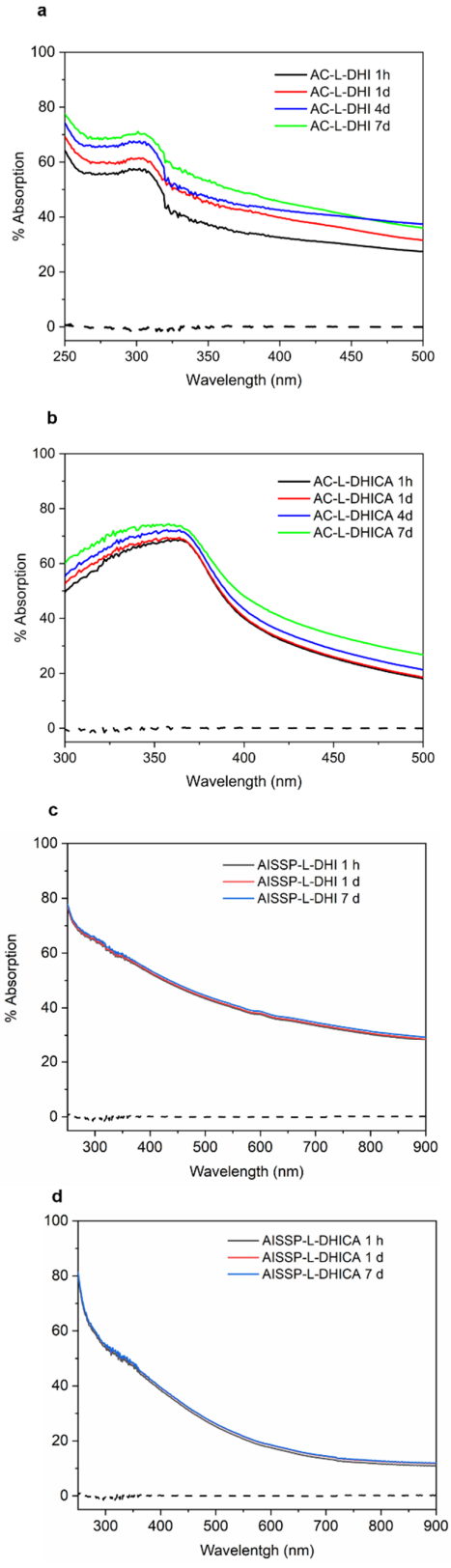


**Figure 4.** UV-Vis absorption spectra of **(a)** AC-L-DHI, **(c)** AISSP-L, **(b)** AC-L-DHICA and **(d)** AISSP-L-DHICA films respectively. The dotted black line shows the UV-Vis absorption spectrum of fused silica (background substrate).

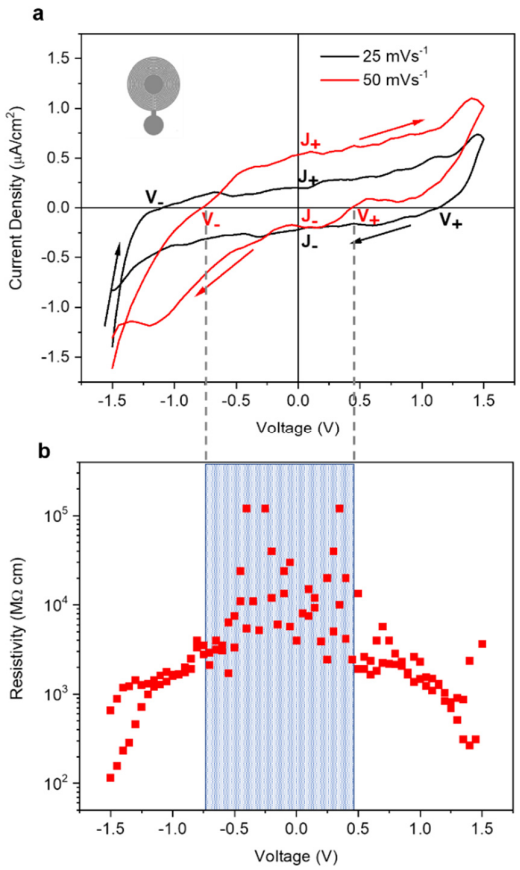


**Figure 5.** AC-L-DHICA films **(a)** J-V hysteresis at different scan rates on circular interdigitated Ti/Au electrodes (schematic of electrodes geometry is in inset of **(a)**). In **(a)** the third J-V cycle is shown. In **(b)** Resistivity at 50 $mVs^{-1}$.

The UV-Vis spectrum of AISSP-L-DHI is characteristic of the polymerized form (i.e. broadband) already after 1 h from fabrication. On the other hand, in AISSP-L-DHICA spectra, the presence of a small feature at around 351 nm after one week at ambient conditions, suggests a slower polymerization rate than that of AISSP-L-DHI films.

## Electrical characterization of DHICA- and DHI-based films

The electrical response of AC-L-DHICA and AC-L-DHI films (respectively Figure 5(a) and Figure S6, SI) features hysteresis behavior in the current density voltage curves (J-V) obtained sweeping the voltage at 25 $mVs^{-1}$ and 50 $mVs^{-1}$ in vacuum conditions (see Experimental). Hysteresis curves, akin to those we report here, were also observed in a few conjugated organic polymer-based memory devices (e.g. 3-(6-methoxylhexyl) thiophene (P6Ome)[42], poly (3,4-ethylenedioxythiophene):poly(4-styrenesulfonate)[43] (PEDOT:PSS) and synthetic eumelanin films[11]).

We observe that hysteresis area and parameters $J_+(V = 0)$, $J_-(V = 0)$, $V_+(J = 0)$, $V_-(J = 0)$ depend on voltage scan rate (Figure 5 (a), Figure S6 (a) and Table S4, SI). Indeed, when changing the voltage scan rate from 25 $mVs^{-1}$ to 50 $mVs^{-1}$ we observe an increase of the hysteresis areas, paralleled by a decrease of $V_+(J = 0)$ and $V_-(J = 0)$ (Table S4, SI).

Regardless of the voltage scan rate, the hysteresis curves are asymmetrical (i.e. current density is higher in the negative voltage region than in the positive one). Furthermore, AC-L-DHICA hysteresis exhibits a broad peak centered around -1.1 V at 50 $mVs^{-1}$ not observable at 25 $mVs^{-1}$ which could be due to diffusion limited proton-related phenomena. This peak is absent for the hysteresis of AC-L-DHI at any voltage scan rate (Figure 5(a) and Figure S6, SI).

The formation of *space charge layers* (i.e. excess of electrons and/or holes in a region of space) in presence of an electric field, followed by de-trapping of charge carriers from traps at structural defect sites, may explain the electrical hysteresis of our films.[11]

Structural defects originate from disruption of hydrogen bond networks, steric hindrance, weaker-than-average interchain interactions, higher (lower)-than-average conjugated molecular segments (i.e. electronic coupling)[44,45]. The build-up of space charge layers of different densities at the metal electrodes/film interfaces would justify the asymmetry of the hysteresis. The higher amount of charge stored in our films at 25 $mVs^{-1}$ than at 50 $mVs^{-1}$ supports the build-up of denser space charge layers at slower voltage scan rates (Table S4, SI and Experimental). Assuming space charge layer formation in the presence of an electric field, charge carriers could hop from one defect to another via charge trapping/releasing mechanisms. The resistivity-voltage characteristics (ρ-V) of our films show significant variations in the region of the plot where $V_-(J = 0) \leq V \leq V_+(J = 0)$ (blue shaded region, Figure 5(b)). This region corresponds to the portion of the plot where $J_-(V = 0)$ and $J_+(V = 0)$ are detected (Figure 5(b) and Figure S6 (b), SI). The presence of oscillations in the ρ-V characteristics of a few organic conjugated polymers, has been considered as evidence of charge transport taking place via trapping/releasing mechanisms[11,43]. These observations suggest that the current densities $J_-(V = 0)$ and $J_+(V = 0)$ would originate from combined effects of charge carrier trapping/releasing mechanisms.

## 4. CONCLUSIONS

In conclusion, we show that films spin-coated on $SiO_2$ from solutions of eumelanin DHI and DHICA building blocks (monomers) dramatically *evolve over time* as a function of the environmental conditions. Atomic force microscopy (AFM) images of DHI-based films kept in the dark show the formation of fern-like structures, explained by diffusion-limited aggregation. Further, if samples are not protected from light, pillar-like and crystal-like aggregates form on ferns over different time scales.

On the other hand, AFM images of DHICA-based films show the formation of rod-shaped structures, attributed to Ostwald ripening.

When *exposed to ammonia (catalyst for the solid-state polymerization), DHI- and DHICA-based films feature polymorphism*: in the case of DHI, we observe fibers, sphere-like structures and flat regions, whereas in the case of DHICA-based films sphere-like and shell-like structures as well as rods.

Infrared spectroscopy suggests a combination of physical (π-π stacking and hydrogen bonding) and chemical (new covalent bonds) interactions occurring as a function of time, after deposition. The *exposure to ammonia vapors* of *DHI* causes the *oxidation* of the films, a crucial step to form new covalent bonds (polymerization). Conversely, there are indications that ammonia does not oxidize DHICA to the same extent as DHI.

The evolution of the optical HOMO-LUMO gap of both DHI and DHICA films, evaluated from the UV-Vis spectra at different stages after deposition, cannot exclude the hypothesis of π-electron delocalization.

After the physicochemical surveys we explored the electrical response of DHI and DHICA-based films. We show that the current-voltage response, in vacuum atmosphere, is an electrical *hysteresis* which we attribute to charge carrier trapping/de-trapping mechanisms, expected in organic electronic materials.

Work is in progress to shed light onto a possible further degree of freedom in our study, namely the aging of the DHI and DHICA powders.

All in all, our results are paramount for understanding the structure-property relationships in eumelanin, which is a fundamental step to achieve eumelanin films of device quality. Our study is a step in the establishment of a *phase diagram* that correlates eumelanin film processing parameters, morphology, and functional properties. The creation of this diagram is necessary for exploitation of the full technological potential of usually disordered bio-sourced organic electronic materials, well beyond eumelanin.

## AUTHOR INFORMATION


### Corresponding Author

**Clara Santato** - *Department of Engineering Physics, Polytechnique Montreal, C.P. 6079, Succ. Centre-ville, Montréal, QC, H3C 3A7, Canada;*
Email: clara.santato@polymtl.ca

### Authors

**Manuel Reali** - *Department of Engineering Physics, Polytechnique Montreal, C.P. 6079, Succ. Centre-ville, Montréal, QC, H3C 3A7, Canada;*

**Anthony Camus** - *Department of Engineering Physics, Polytechnique Montreal, C.P. 6079, Succ. Centre-ville, Montréal, QC, H3C 3A7, Canada;*

**Guillaume Beaulieu** - *Department of Engineering Physics, Polytechnique Montreal, C.P. 6079, Succ. Centre-ville, Montréal, QC, H3C 3A7, Canada;*

**Jordan De Angelis** - *Department of Electronic, Electrical and Information Engineering (DEI), University of Bologna, Viale del Risorgimento 2, 40136, Italy;*

**Christian Pellerin** - *Département de chimie, Université de Montréal, C.P. 6128, Succ. Centre-ville, Montréal, QC, H3C 3J7, Canada;*

**Alessandro Pezzella** - *Department of Physics "Ettore Pancini", University of Naples "Federico II", Complesso Universitario Monte S. Angelo, Via Cintia 1, 80126, Naples, Italy.*


## NOTES

The authors declare no competing financial interest

## ACKNOWLEDGMENTS


The authors thank Y. Drolet and P. Moraille for technical support. C. Santato acknowledges financial support from NSERC (Discovery grant and Strategic Network in Green Electronics grant number: NETGP 508526-17), FQRNT (Team grant) and MESI-Quebec.


## SUPPORTING INFORMATION

Morphological evolution of AC-DHI films over a period of 1 day, AFM images of AC-DHI films stored 1 day in dark and exposed 1 day to laboratory daylight, AFM images of AISSP-D-DHI films, AFM images of AC-L-DHICA showing the profile of rod-shaped like structures, AFM images of AC-D-DHICA and AISSP-D-DHICA films stored 1 day in the dark, evolution of IR spectra of AC and AISSP DHI and DHICA films over a period of 1 day, J-V hysteresis and resistivity VS voltage response of AC-L-DHI films.

## REFERENCES


(1) Balde, C. P.; Forti, V.; Gray, V.; Kuehr, R.; Stegmann, P. *The Global E-Waste Monitor 2017. Quantities, Flows and Resources.*; United Nations University, 2017.

(2) Irimia-Vladu, M., Glowacki, E. D., Sariciftci, N. S. & Bauer, S. *Green Materials for Electronics*; Irimia-Vladu, Mihai, Eric D. Glowacki, Niyazi S. Sariciftci, S. B., Ed.; Wiley-VCH, Weinheim, Germany, 2018.

(3) Irimia-Vladu, M. "Green" Electronics: Biodegradable and Biocompatible Materials and Devices for Sustainable Future. *Chem. Soc. Rev.* **2014**, *43* (2), 588–610.

(4) Dezidério, S. N.; Brunello, C. A.; Da Silva, M. I. N.; Cotta, M. A.; Graeff, C. F. O. Thin Films of Synthetic Melanin. *J. Non. Cryst. Solids* **2004**, *338–340* (1 SPEC. ISS.), 634–638.

(5) Wünsche, J.; Cardenas, L.; Rosei, F.; Cicoira, F.; Gauvin, R.; Graeff, C. F. O.; Poulin, S.; Pezzella, A.; Santato, C. In Situ Formation of Dendrites in Eumelanin Thin Films between Gold Electrodes. *Adv. Funct. Mater.* **2013**, *23* (45), 5591–5598.

(6) Bronze-Uhle, E. S.; Batagin-Neto, A.; Xavier, P. H. P.; Fernandes, N. I.; De Azevedo, E. R.; Graeff, C. F. O. Synthesis and Characterization of Melanin in DMSO. *J. Mol. Struct.* **2013**, *1047*, 102–108.

(7) De Marchi, F.; Galeotti, G.; Simenas, M.; Ji, P.; Chi, L.; Tornau, E. E.; Pezzella, A.; Macleod, J.; Ebrahimi, M.; Rosei, F. Self-Assembly of 5,6-Dihydroxyindole-2-Carboxylic Acid: Polymorphism of a Eumelanin Building Block on Au(111). *Nanoscale* **2019**, *11* (12), 5422–5428.

(8) Napolitano, A.; Pezzella, A.; Vincensi, M. R.; Prota, G. Oxidative Degradation of Melanins to Pyrrole Acids: A Model Study. *Tetrahedron* **1995**, *51* (20), 5913–5920.

(9) Diao, Y.; Lenn, K. M.; Lee, W. Y.; Blood-Forsythe, M. A.; Xu, J.; Mao, Y.; Kim, Y.; Reinspach, J. A.; Park, S.; Aspuru-Guzik, A.; et al. Understanding Polymorphism in Organic Semiconductor Thin Films through Nanoconfinement. *J. Am. Chem. Soc.* **2014**, *136* (49), 17046–17057.

(10) Riera-Galindo, S.; Tamayo, A.; Mas-Torrent, M. Role of Polymorphism and Thin-Film Morphology in Organic Semiconductors Processed by Solution Shearing. *ACS Omega*

**2018**, *3* (2), 2329–2339.

(11) Ambrico, M.; Cardone, A.; Ligonzo, T.; Augelli, V.; Ambrico, P. F.; Cicco, S.; Farinola, G. M.; Filannino, M.; Perna, G.; Capozzi, V. Hysteresis-Type Current-Voltage Characteristics in Au/Eumelanin/ITO/Glass Structure: Towards Melanin Based Memory Devices. *Org. Electron.* **2010**, *11*, 1809–1814.

(12) Mostert, A. B.; Powell, B. J.; Pratt, F. L.; Hanson, G. R.; Sarna, T.; Gentle, I. R.; Meredith, P. Role of Semiconductivity and Ion Transport in the Electrical Conduction of Melanin. *Proc. Natl. Acad. Sci.* **2012**, *109* (23), 8943–8947.

(13) Reali, M.; Santato, C. Eumelanin: Semiconductor, Protonic Conductor or Mixed Electronic-Ionic Conductor? In *Handbook of Nanoengineering, Quantum Science and Nanotechnology*; Lyshevski, S. E., Ed.; CRC Press, 2019; pp 101–113.

(14) Nam, H. J.; Cha, J.; Lee, S. H.; Yoo, W. J.; Jung, D. Y. A New Mussel-Inspired Polydopamine Phototransistor with High Photosensitivity: Signal Amplification and Light-Controlled Switching Properties. *Chem. Commun.* **2014**, *50* (12), 1458–1461.

(15) Panzella, L.; Gentile, G.; D'Errico, G.; Della Vecchia, N. F.; Errico, M. E.; Napolitano, A.; Carfagna, C.; D'Ischia, M. Atypical Structural and π-Electron Features of a Melanin Polymer That Lead to Superior Free-Radical-Scavenging Properties. *Angew. Chemie - Int. Ed.* **2013**, *52* (48), 1–5.

(16) Chen, C. T.; Chuang, C.; Cao, J.; Ball, V.; Ruch, D.; Buehler, M. J. Excitonic Effects from Geometric Order and Disorder Explain Broadband Optical Absorption in Eumelanin. *Nat. Commun.* **2014**, *5* , 1–10.

(17) Tran, M. L.; Powell, B. J.; Meredith, P. Chemical and Structural Disorder in Eumelanins: A Possible Explanation for Broadband Absorbance. *Biophys. J.* **2006**, *90* (3), 743–752.

(18) D'Ischia, M.; Napolitano, A.; Pezzella, A.; Meredith, P.; Sarna, T. Chemical and Structural Diversity in Eumelanins: Unexplored Bio-Optoelectronic Materials. *Angew. Chemie - Int. Ed.* **2009**, *48*, 3914–3921.

(19) Antidormi, A.; Melis, C.; Canadell, E.; Colombo, L. Understanding the Polymerization Process of Eumelanin by Computer Simulations. *J. Phys. Chem. C* **2018**, *122* (49), 28368–28374.

(20) Meng, S.; Kaxiras, E. Theoretical Models of Eumelanin Protomolecules and Their Optical Properties. *Biophys. J.* **2008**, *94* (6), 2095–2105.

(21) Xiao, M.; Chen, W.; Li, W.; Zhao, J.; Hong, Y. Elucidation of the Hierarchical Structure of Natural Eumelanins. *J. R. Scociety Interface* **2018**, *15*, 1–10.

(22) Molteni, E.; Cappellini, G.; Onida, G.; Mula, G. Extensive Stacking of DHI-like Monomers as a Model of out-of-Plane Complexity in Eumelanin Protomolecules: Chemical and Structural Sensitivity of Optical Absorption Spectra. *Chem. Phys.* **2019**, *524*, 92–100.

(23) Watt, A. A. R.; Bothma, J. P.; Meredith, P. The Supramolecular Structure of Melanin. *Soft Matter* **2009**, *5* (19), 3754–3760.

(24) Büngeler, A.; Hämisch, B.; Huber, K.; Bremser, W.; Strube, O. I. Insight into the Final Step of the Supramolecular Buildup of Eumelanin. *Langmuir* **2017**, *33* (27), 6895–6901.

(25) Pezzella, A.; Barra, M.; Musto, A.; Navarra, A.; Alfè, M.; Manini, P.; Parisi, S.; Cassinese, A.; Criscuolo, V.; D'Ischia, M. Stem Cell-Compatible Eumelanin Biointerface Fabricated by Chemically Controlled Solid State Polymerization. *Mater. Horizons* **2015**, *2* (2), 212–220.

(26) Pezzella, A.; Oscurato, S.; Formisano, F.; Delsio, C.; d'Ischia, M.; Maddalena, P.; Manini, P.; Migliaccio, L.; Gesuele, F. Spontaneous Wrinkle Emergence in Nascent Eumelanin Thin Films. *Soft Matter* **2019**, 9261–9270.

(27) Halsey, T. C. Diffusion-Limited Aggregation: A Model for Pattern Formation. *Phys. Today* **2000**, *53* (11), 36–41.

(28) Deegan, R. D.; Bakajin, O.; Dupont, T. F.; Huber, G.; Nagel, S. R.; Witten, T. A. Capillary Flowas the Cause of Ring Stains Fromdried Liquid Drops. *Nature* **1997**, *389* (23), 827–829.

(29) Huang, J. S.; Sung, J.; Eisner, M.; Moss, S. C.; Gallas, J. The Fractal Structure and the Dynamics of Aggregation of Synthetic Melanin in Low pH Aqueous Solutions. *J. Chem. Phys.* **1989**, *90* (1), 25–29.

(30) Bridelli, M. G. Self-Assembly of Melanin Studied by Laser Light Scattering. *Biophys. Chem.* **1998**, *73* (3), 227–239.

(31) Mukherjee, R.; Sharma, A. Instability, Self-Organization and Pattern Formation in Thin Soft Films. *Soft Matter* **2015**, *11* (45), 8717–8740.

(32) Baldan, A. Progress in Ostwald Ripening Theories and Their Applications to Nickel-Base Superalloys. Part I: Ostwald Ripening Theories. *J. Mater. Sci.* **2002**, *37* (11), 2171–2202.

(33) Raposo, M.; Ferreira, Q.; Ribeiro, P. a. A Guide for

Atomic Force Microscopy Analysis of Soft-Condensed Matter. *Mod. Res. Educ. Top. Microsc.* **2007**, 758–769.

(34) Roldán, M. L.; Centeno, S. A.; Rizzo, A. An Improved Methodology for the Characterization and Identification of Sepia in Works of Art by Normal Raman and SERS, Complemented by FTIR, Py-GC/MS, and XRF. *J. Raman Spectrosc.* **2014**, *45* (11–12), 1160–

(35) Centeno, S. A.; Shamir, J. Surface Enhanced Raman Scattering (SERS) and FTIR Characterization of the Sepia Melanin Pigment Used in Works of Art. *J. Mol. Struct.* **2008**, *873* (1–3), 149–159.

(36) Kiran, G. S.; Jackson, S. A.; Priyadharsini, S.; Dobson, A. D. W.; Selvin, J. Synthesis of Nm-PHB (Nanomelanin-Polyhydroxy Butyrate) Nanocomposite Film and Its Protective Effect against Biofilm-Forming Multi Drug Resistant Staphylococcus Aureus. *Sci. Rep.* **2017**, *7* (1), 1–13.

(37) Okuda, H.; Wakamatsu, K.; Ito, S.; Sota, T. Possible Oxidative Polymerization Mechanism of 5,6-Dihydroxyindole from Ab Initio Calculations. *J. Phys. Chem. A* **2008**, *112* (44), 11213–11222..

(38) Alves, G. G. B.; Lavarda, F. C.; Graeff, C. F. O.; Batagin-Neto, A. Reactivity of Eumelanin Building Blocks: A DFT Study of Monomers and Dimers. *J. Mol. Graph. Model.* **2020**, *98*, 107609.

(39) D'Ischia, M.; Crescenzi, O.; Pezzella, A.; Arzillo, M.; Panzella, L.; Napolitano, A.; Barone, V. Structural Effects on the Electronic Absorption Properties of 5,6-Dihydroxyindole Oligomers: The Potential of an Integrated Experimental and DFT Approach to Model Eumelanin Optical Properties. *Photochem. Photobiol.* **2008**, *84* (3), 600–607.

(40) Campbell, D.; Pethrick, R. A.; White, J. R. Ultraviolet – Visible Spectroscopy. *Polym. Charact.* **2018**, 58–66.

(41) Ju, K.-Y.; Fischer, M. C.; Warren, W. S. Understanding The Role Of Aggregation In The Broad Absorption Bands Of Eumelanin. *ACS Nano* **2018**, *12*, 12050–12061.

(42) Majumdar, H. S.; Bandyopadhyay, A.; Bolognesi, A.; Pal, A. J. Memory Device Applications of a Conjugated Polymer: Role of Space Charges. *J. Appl. Phys.* **2002**, *91* (3), 2433–2437.

(43) Lin, Y. J. Hysteresis-Type Current-Voltage Characteristics of Indium Tin Oxide/Poly (3,4-Ethylenedioxythiophene) Doped with Poly (4-Styrenesulfonate)/Indium Tin Oxide Devices. *J. Appl. Phys.* **2008**, *103* (6), 1–5.

(44) A. Salleo. Electronic Traps in Organic Semiconductors, Ch. 14. In *Organic Electronics: Emerging Concepts and Technology*; Cicoira, F., Santato, C., Ed.; Wiley-VCH, 2013; pp 341–373.

(45) Matta, M.; Pezzella, A.; Troisi, A. Relation between Local Structure, Electric Dipole, and Charge Carrier Dynamics in DHICA Melanin: A Model for Biocompatible Semiconductors. *J. Phys. Chem. Lett.* **2020**, *11* (3), 1045–1051.

(46) Edge, R.; D'Ischia, M.; Land, E. J.; Napolitano, A.; Navaratnam, S.; Panzella, L.; Pezzella, A.; Ramsden, C. A.; Riley, P. A. Dopaquinone Redox Exchange with Dihydroxyindole and Dihydroxyindole Carboxylic Acid. *Pigment Cell Res.* **2006**, *19* (5), 443–450.

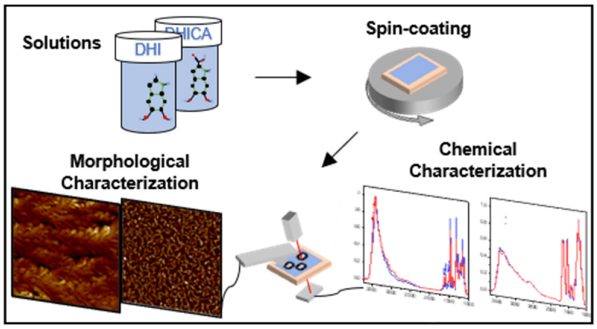


ToC Abstract